A Parallel Computing Based Spectrum Sensing Approach for Signal Detection under Conditions of Low SNR and Rayleigh Multipath Fading

Feng Ge and Charles W. Bostian
Wireless @ Virginia Tech
Center for Wireless Telecommunications (CWT)
466 Whittemore Hall, Virginia Tech, Blacksburg, VA 24061, USA
Email: {gef, bostian}@vt.edu
Phone: 1-540-231-5096
Fax: 1-540-231-3362

***Abstract*—Quickly and accurately detecting signals over a wide frequency range under conditions of low SNR and multipath fading is one of the most challenging requirements for dynamic spectrum access devices. The cyclostationary feature detection method is attractive for detecting primary users because of its ability to distinguish between modulated signals, interference, and noise at low SNRs. However, a key issue of cyclostationary signal analysis is the high computational cost arising from the large number of required complex convolution operations. This complexity increases in proportion to signal bandwidth if frequency resolution is held constant.**

To reduce the computation requirements, we use parallel computing in cyclostationary feature analysis running on a Cell Broadband Engine (Cell BE). Specifically, we parallelized the FFT accumulation method (FAM) algorithm to calculate spectral correlation functions (SCF) on four available Synergistic Processing Elements in a PlayStation 3. We analyze our algorithm's computational speedup on a Cell BE compared to a GPP based version.

We analyze the impact of AWGN and Rayleigh multipath fading on signals' SCF features in the bi-frequency plane (with axes of cyclic-frequency and frequency). Next, we design a spectrum sensing algorithm which uses the distinct SCF pattern of each modulated signal to detect its existence. We run this algorithm on simulated signals including M-ary Phase-shift keying (PSK), Frequency-shift keying (FSK), Quadrature amplitude modulation (QAM), and PSK based Orthogonal frequency-division multiplexing (OFDM) under conditions of multipath fading and different levels of SNR. We give numerical results for the detector's performance.

Keywords: Dynamic Spectrum Access, Cyclostationary Features, Signal Detection, Parallel Computing.

I. Introduction

The limited available spectrum and its inefficient use necessitate a new communication paradigm like Dynamic Spectrum Access (DSA) and cognitive radio networks [1] to opportunistically exploit the existing wireless spectrum. The first and foremost requirement for DSA implementations is to guarantee non-interference to primary users. This implies communication nodes with two capabilities: (1) to sense signals over a wide frequency range even at a very low SNR level and various other conditions; (2) to switch quickly to other possible vacant channels upon in-band primary signals' appearance. The first condition is very challenging, for example, the National Association of Broadcasters requires white space devices accurately to detect TV broadcasts at -116 dBm [2], which may be under the noise floor. In addition, the detection performance should hold even under hostile conditions like shadowing, fading, and multipath [3].

Cyclostationary feature detection has advantages for spectrum sensing because of its ability to separate the Signal of Interest (SOI) from noise and/or interference in the spectral correlation plane [4]. It is well suited for signal detection and modulation recognition, signal parameter estimation, and the design of communication signals and systems. Unfortunately, the computational complexity of cyclic spectral analysis (which far exceeds that of conventional spectral analysis) limits its use as a signal and system analysis tool. One way to attack the computational complexity is to use a parallel algorithm and implement it on parallel computers. Cell BE [5], a specially designed single-chip multiprocessor with low-cost and high parallel computing ability, provides this opportunity. It operates on a shared, coherent memory supporting one Power Processor Element (PPE) acting as the controller for the eight Synergistic Processing Elements (SPEs) processors designed especially for computation-intensive tasks. Cell BE's peak performance for single precision calculation is larger than 200 GFlops [6] and it provides a software development kit for parallel computing. In this paper, we use a PlayStation 3 with six usable SPEs to implement the computationally efficient algorithm FFT Accumulation Method (FAM) in order to estimate the Spectral Correlation Function (SCF) [7]. Specifically, we parallelize the FAM algorithm on four SPEs to execute the computation intensive part and use the PPE to coordinate SPEs. We also used the data level parallelism supported by Single Instruction, Multiple Data (SIMD) and Vector Multimedia Extension (VMX) instructions and other acceleration techniques like Direct Memory Access (DMA), loop unrolling, double-buffering, etc. [8]. This paper compares the computational complexity of running an SCF algorithm

978-1-4244-2017-9/08/$25.00 ©2008 IEEE

for different signal bandwidths, both sequentially on a GPP, and in parallel on a Cell BE. We analyze our algorithm's computational speedup on a Cell BE compared to a GPP based version for different bandwidths of signals.

In our experiment, we simulate different modulated signals under conditions of multipath fading and different levels of SNR. The signal types include M-ary Phase-shift keying (PSK), Frequency-shift keying (FSK), Quadrature amplitude modulation (QAM), and M-ary PSK based Orthogonal frequency-division multiplexing (OFDM). In the bi-frequency plane (with axes of cyclic-frequency and frequency), we investigated the above signals' SCF distinct features under multipath fading and different levels of SNR. All the signals use a root raised cosine filter for pulse shaping and are up-converted to an RF band. Based on cyclostationary features of different modulated signals, we designed a signal detection algorithm which can detect modulated signals in the bi-frequency plane. Numerical performance of the detector is given for different signals at different SNRs and multipath fading environments. To simulate a real signal detection scenario, we assume that the SOI is completely unknown including its frequency and modulation type. Our signal detection algorithm has to scan the whole RF band to identify any signal's presence.

II. Signal Sensing Approach

The goal of signal detection usually is to detect SOI over a wide frequency range under conditions of low SNR, interference, and other dynamic wireless environments. This obviously applies to DSA implementations where signal detection mostly occurs in a band limited domain. In a digital domain, this means that a finite length of a high frequency signal is first down-converted into some IF band, and then numerical methods are used to discover the presence of any signals. Suppose that x is the sequence of collected data, the detection problem (with only AWGN) can be formulated through the hypothesis test:

$$\begin{aligned} H_0 &: x = n \\ H_1 &: x = s + n \end{aligned} \tag{1}$$

where s is the unknown signal to be detected and n is an AWGN. There are two types of error [9]: (1) false positive means the error of detecting a signal where none is present; (2) false negative means the error of missing a signal where there is one. The two errors are mostly correlated, and a receiver operating characteristic (ROC) curve can be used to analyze the two error probabilities for different detection parameter settings like thresholds [9].

This hypothesis test can be expanded for detecting multiple signals, but more complicated algorithms are needed [9]. In addition, better signal models are needed to include interference, multipath, fading, and other dynamic wireless environments [10].

A. Cyclostationary Spectral Analysis

Modulated signals have built-in periodicity, characterized as cyclostationary. This information can be used for detecting a random signal with a particular modulation type in the presence of background noise and other modulated signals. Cyclostationary signals exhibit correlation between widely separated spectral components due to the spectral redundancy caused by periodicity. A signal process $x(n)$ is said to be cyclostationary in a wide sense if its mean and autocorrelation are periodic with a period T_0, i.e.,

$$\begin{aligned} M_x(t + T_0) &= M_x(t) \\ R_x(t + T_0, \tau) &= R_x(t, \tau) \end{aligned} \tag{2}$$

for all t and τ. Therefore, by assuming that the Fourier series expansion of $R_x(t, \tau)$ converges to itself, we can write [11]:

$$R_x(t, \tau) = \sum_{n=-\infty}^{+\infty} R_x^{\frac{n}{T_0}}(\tau) e^{i2\pi \frac{n}{T_0} t} \tag{3}$$

where the Fourier coefficients

$$R_x^{\frac{n}{T_0}} = \frac{1}{T_0} \int_{-\frac{T_0}{2}}^{\frac{T_0}{2}} R_x(t, \tau) e^{-i2\pi \frac{n}{T_0} t} dt \tag{4}$$

are referred to as cyclic autocorrelation functions and the frequencies $\{\frac{n}{T_0}\}_{n \in Z}$ are called cycle frequencies. Let α represent cycle frequency when the spectral correlation function (SCF) is defined as:

$$S_x^{\alpha}(f) = \int_{-\infty}^{\infty} R_x^{\alpha}(\tau) e^{-i2\pi f \tau} d\tau \tag{5}$$

There are generally two methods to estimate the signal SCF: frequency smoothing and time smoothing [12]. Time smoothing algorithms are considered to be more computationally efficient for general cyclic spectral analysis [12]. Given the signal $x(n)$, all time smoothing algorithms are based on the time smoothed cyclic cross periodogram:

$$S_x^{\alpha}(n, f)_{\Delta t} = \frac{1}{T} \langle X_T(n, f + \alpha/2) X_T^*(n, f - \alpha/2) \rangle_{\Delta t} \tag{6}$$

where $X_T(n, f + \alpha/2)$, also called complex demodulators, is the spectral components of signal $x(n)$. * is the complex conjugate operator. The cyclic cross periodogram is calculated by using a data tapering window of length T seconds sliding over the data for a time span of Δt seconds. Mathematically, computation of the complex demodulators is expressed as

$$X_T(n, f) = \sum_{r=-\frac{N'}{2}}^{\frac{N'}{2}} a(r) x(n - r) e^{-i2\pi f (n-r) T_s} \tag{7}$$

where $a(r)$ is a data tapering window of length $T = N' T_s$ seconds, T_s is the sample interval, and f_s is the sampling frequency.

After the complex demodulate has been computed, it is correlated with its conjugate over a time span of Δt seconds. The correlation operation is expressed as

$$S_x^{\alpha}(n, f)_{\Delta t} = \sum_{r=0}^{N-1} X_T(r, f_1) X_T^*(r, f_2) g(n - r) \tag{8}$$

where $g(n)$ is a data tapering window of width $\Delta t = NT_s$ seconds, and $f = (f_1 + f_2)/2$ and $\alpha = f_2 - f_1$.

It is shown in [13] that the time smoothed cyclic cross periodogram converges to the spectral correlation function in the limit, as $\Delta t \rightarrow \infty$ followed by $f \rightarrow 0$, if the time windows $a(n)$ and $g(n)$ are properly normalized. Therefore, if $\sum_n a^2(n) = \sum_n g^2(n) = 1$, we have

$$\lim_{\Delta f \rightarrow 0} \lim_{\Delta t \rightarrow \infty} S_x^\alpha(n, f)_{\Delta t} = S_x^\alpha(f) \tag{9}$$

B. FFT Accumulation Method (FAM) Algorithm

The signal SCF can be estimated by Eq. (6) by two stages: first the complex demodulate of $x(n)$ is calculated through Eq. (7), then the demodulate $X_T(n, f)$ is correlated over a time period of Δt seconds. The computational efficiency of this algorithm can be improved by decimating $X_T(n, f)$. For example, it only gets every other $L (L < N')$ sample for the second stage FFT. Therefore, Eq. (8) is modified to

$$S_x^\alpha(nL, f)_{\Delta t} = \sum_{r=0}^{\frac{N}{L}-1} X_T(rL, f_1) X_T^*(rL, f_2) g(n - r) \tag{10}$$

On the other hand, considering the frequency shifting for the second stage of SCF estimation, for example, from α to $\alpha + \varepsilon$, Eq. (8) becomes

$$S_x^{\alpha+\varepsilon}(n, f)_{\Delta t} = \sum_{r=0}^{N-1} X_T(r, f_1) X_T^*(r, f_2) g(n - r) e^{-i2\pi\varepsilon r T_s} \tag{11}$$

FAM is a computationally efficient algorithm to combine Eq. (10) and Eq. (11). It further quantizes ε into $\varepsilon = q\alpha$ [12]. Therefore, the demodulate correlation stage can be implemented in Fast Fourier Transform (FFT) too. The discrete S value $S_x^{\alpha_i + q\Delta\alpha}(nL, f_i)_{\Delta t}$ at the point with the cyclic frequency of $\alpha_i + q\Delta\alpha$ and the signal frequency of f_i in the bi-frequency plane is shown in Eq. (12)

$$S_x^{\alpha_i + q\Delta\alpha}(nL, f_i)_{\Delta t} = \sum_{r=0}^{P-1} X_T(rL, f_k) X_T^*(rL, f_l) \; g(n - r) e^{-\frac{i2\pi rq}{P}} \tag{12}$$

where α_i represents discrete cyclic frequency channels, $\Delta\alpha$ indicates cyclic frequency resolution in each channel and q is an integer; together $\alpha_i + q\Delta\alpha$ represents a discrete cyclic frequency value. f_k and f_l are the frequency values in correlating two spectral components; they decide the value of α_i by $\alpha_i = f_k - f_l$. Furthermore, L is a decimation factor for channelization in the frequency domain, P equals $\frac{N-N'}{L} + 1$ where N is the total number of samples and N' is the number of samples used to calculate each complex demodulator $X_T(rL, f_k)$. The choice of N' must take into consideration that the time-frequency resolution product $\frac{N}{N'}$ must satisfy $\frac{N}{N'} \gg 1$ for a statistically reliable measurement [12] and that N' is large enough to obtain the desired frequency resolution. L is usually chosen to be less than or equal to $\frac{N'}{4}$ [14]. More details about Eq. (12) and its variables' meaning are available in [12], [14], [15].

Essentially, the FAM algorithm can be described by Figure 1: the input signal is formed as an array with rows which are N' points long with each succeeding row's starting point offset from the previous row starting position by L samples in the original sample sequence (input channelization). A window is applied across each row which is then Fast Fourier transformed and down converted to the baseband. The resulting array's columns represent constant frequencies, which are point-wise multiplied with the conjugate of other columns; the final stage is another round of FFT.

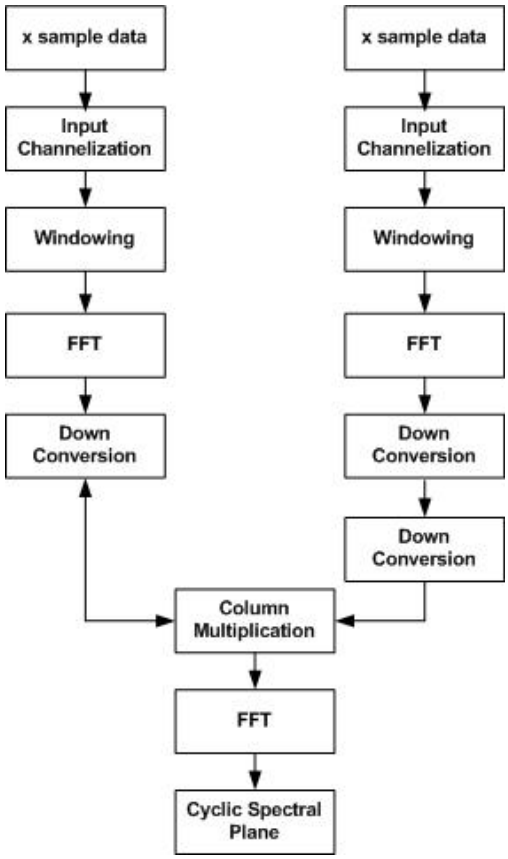

Fig. 1. Sequential implementation of FAM algorithm [14].

In [14], FAM is implemented in C on the general purpose processor. A Matlab version is also given by [16]. Following the above algorithm, the computation cost for a signal sequence with N samples is given by the expression shown in (13). Here, the first item represents the windowing, downconversion, and column multiplication computational cost, and the second item represents the two stages of FFTs computational cost which dominates the total value.

$$(3 + 2{*}N') {*} \frac{NN'}{L} + \frac{NN'}{L} (\log_2 N' + N' \log_2 (\frac{N}{L})) \tag{13}$$

Considering the above parameter selection and the Nyquist Sampling Theorem, the computational requirement to cover a frequency range with 10 MHz bandwidth within one second is on the order of 1 Giga Floating point operations per second (GFlops) for a frequency resolution of 50Hz [15]. The computational cost is too high for current general purpose

processors (GPPs). To demonstrate the computational requirement, we run the FAM algorithm for a different number of samples on an Intel Duo Core processor with 2.40 GHz CPU and 2 GB memory. Correspondingly, the amount of samples can represent different frequency resolutions given different parameter settings, as shown in Table I, which also contains the time to accomplish the computation.

TABLE I
SERIAL FAM COMPUTING TIME.

N (samples)	N'	L	P	Resolution (Hz)	Time (s)
2^{18}	2^8	2^6	2^{12}	2^6	60.0
2^{17}	2^8	2^6	2^{11}	2^7	30.55
2^{16}	2^8	2^6	2^{10}	2^8	13.28
2^{15}	2^7	2^5	2^{10}	2^9	3.39
2^{14}	2^6	2^4	2^{10}	2^{10}	0.896
2^{13}	2^5	2^3	2^{10}	2^{11}	0.273

C. Parallel FAM algorithm on the Cell BE

Although cyclostationary feature analysis has the advantage of being able to differentiate modulated signals from noise, a key issue is the computational complexity associated with the calculation of a complete spectral correlation density function [7], [17]. This calculation is the main computing challenge in signal detection methods based on cyclostationary features. Even the computationally efficient algorithm FAM requires several seconds on a fast GPP, as shown in Section II-B and Table I. Just based on such signal detection, it is not feasible for DSA implementations. For example, DARPA's XG system requires 0.5 second switching upon a primary signal's appearance [1]. Parallel computation can be used to attack this problem and two parallel computation structures are proposed for the Digital Frequency Smoothing Method in [7]. In addition, GPPs are not optimized for scientific computation since they are designed to run multiple general purpose tasks by using operating system and a memory hierarchy [18].

We have designed a parallel FAM algorithm on a PlayStation 3 powered by the specially designed single-chip multiprocessor Cell BE with low-cost and high parallel computing ability [8], [5]. Cell BE uses a conventional high performance PowerPC core, also called the PPE, that controls eight simple SIMD cores known as SPEs. These SPEs are designed for computation- intensive tasks. To fully utilize Cell BE's capacity, it is required to distribute efficiently and effectively any computational task over the usable SPEs. This should take into account the Cell BE communication mechanism and memory bandwidth, SPEs' local memory size, SIMD operation, and computational models, etc. [8]. In our signal sensing approach, the FAM algorithm is parallelized to utilize four usable SPEs and the one PPE in a PlayStation 3. As shown in Eq. (13), the dominating computation cost lies in two stages of FFTs, which are also our focus for parallelization. The first stage has approximately N/L FFTs with the size of N', where the second stage has approximately N'^2 FFTs with the size of L. As mentioned in Section II-B, we have $\frac{N}{N'} \gg 1$, $N' \gg 1$ and $L \leq \frac{N'}{4}$. Therefore, the FFT size in the first stage is moderate, while the FFT size in the second stage is slightly larger. To estimate both sizes, we use an example. To cover 4MHz bandwidth (BW) with the resolution of 40Hz, we can get a data sample rate of 10Msps to have some frequency margin, N is 262144, and we can have $N' = 256, L = 64$,and $\frac{N}{L} = 4096$. Considering the SPE's Local Store size (256 KB), the above two FFT sizes can usually be accommodated by one SPE if the covered frequency BW is within tens of MHz. Therefore, our algorithm will distribute FFTs equally among 4 usable SPEs and the PPE. To reduce the communication cost, we choose a slightly larger N' so that each SPE can receive larger continuous data chunks each time, and the total number of parallel tasks is also reduced. The data independency among FFTs in either stage also enables our parallel mechanism.

Specifically, as shown in Figure 2, we parallelize the FAM used in [14]. It processes the input channelization on the PPE, then parallelizes $\frac{N-N'}{L}+1$ FFTs operations into 4 SPEs which also run windowing and down conversion before and after FFT operation respectively. Then the data are sent back to the PPE for column multiplications which are partitioned and executed by the second stage of FFTs on 4 SPEs. Finally the data are post-processed in the PPE. All the data exchange between the PPE and SPEs is done through double buffered Direct Memory Access (DMA) [8] which reads 128 bytes of data for each DMA command and asynchronously execute a list of DMA transfers while the SPE operates on previously transferred data.

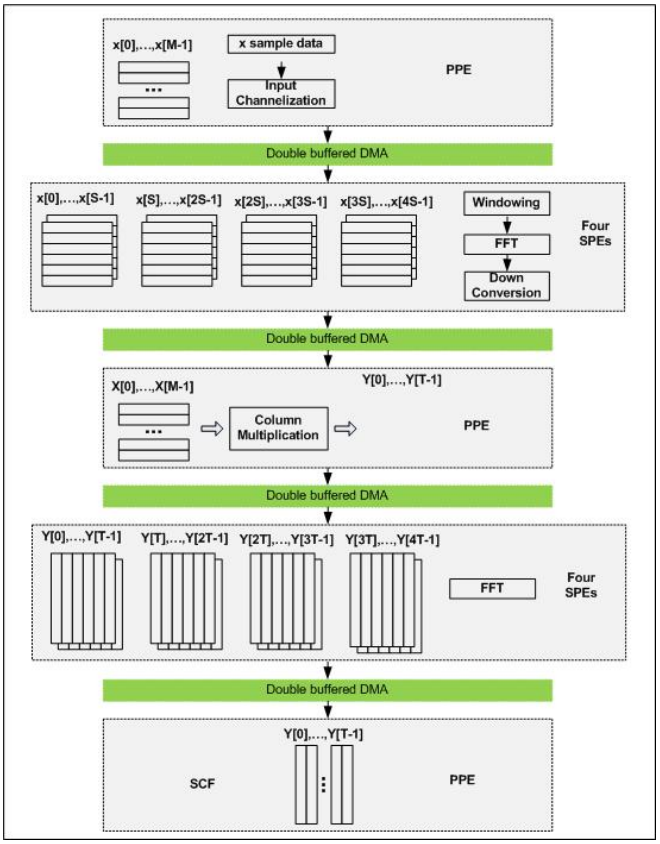

Fig. 2. Parallelize FAM algorithm on the PlayStation 3.

As shown above, we discussed the parallelism granularity analysis at the task level supported by 4 SPEs and the PPE. Another level is the data level parallelism supported by SIMD and VMX instructions. Everything in the SPEs is done in quadword (16 byte) granularity. For single-precision floats this corresponds to 4 way SIMD operation. We use the modified stride-by-1 FFT algorithm proposed in [19] so that the FFT array can be partitioned naturally, without data rearrangement, into vectors that can be executed in parallel by SIMD instructions. Our other implementation details include loop unrolling, pre-computed sin and cos arrays for FFT, double-buffering, using system-specific large TLB pages, etc. As a result, we need 0.446 second to accomplish the parallel FAM on an 8 MHz BW signal at frequency resolution of 512 Hz (32768 samples) which is around 7.6 times faster on a serial FAM on the previous GPP (3.39 seconds).

D. Noise and Multipath Impact on Signals' SCF

Hidden Markov Model, Neural Network, and other pattern recognition algorithms are proposed to classify several modulated signals' second order cyclostationary features [20], [21]. However, second order cyclostationary features cannot differentiate among higher order phase-shift keying and quadrature amplitude modulation besides binary phase-shift keying [11]. In addition, theoretically, cyclostationary feature detection has the potential to differentiate modulated signals and noise in low signal to noise ratios [4] because noise doesn't have this feature. However, only a finite length of signal duration is usually used for detection and this impacts the detection performance, as shown in [22]. Besides, multipath fading also has an impact on cyclostationary feature analysis [23]. Therefore, we will first analyze signals' numerical SCF, specifically using FAM algorithm for some finite number of samples, under different levels of SNR and multipath environment. After that we discuss our signal detection method based on SCF.

To analyze the distinct SCF features for different modulated signals in the numerical domain, first we simulate bandlimited signals with different modulations and using root raised cosine pulse shaping (32 order coefficient). Then we add AWGN and multipath fading. A QPSK signal example is shown in Figure 3 which uses 16384 Hz sampling frequency and 1024 Hz carrier frequency.

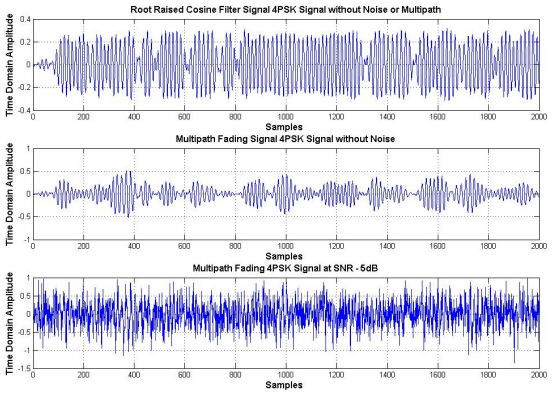

Fig. 3. Simulated QPSK with pulse shaping, AWGN noise, and multipath fading.

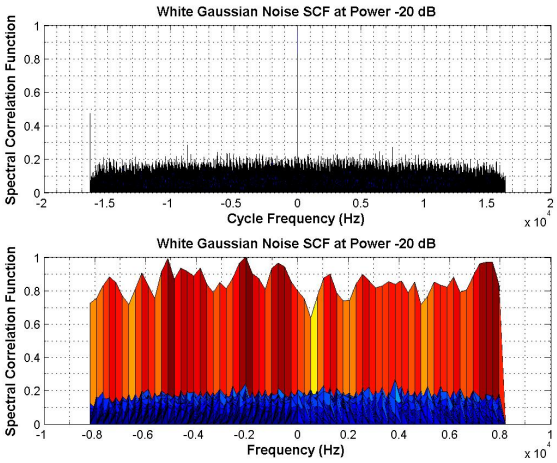

Fig. 4. White Gaussian Noise Spectral Correlation Function at -20 dB power level.

Second, we run the FAM algorithm on different digital signals: M-PSK, M-FSK, M-QAM, and OFDM and find their SCF shape and distribution in the bi-frequency plane, as shown in Figure 8. All the SCF values shown in this paper calculated from the FAM algorithm are normalized magnitude values. All the modulated baseband signals are pulse shaped by a root raised cosine filter before they are up converted to a carrier frequency. For all this section's figures, we use 64 for N', 1024 for P, and 8 for L in the FAM algorithm.

As we can see the SCF is characterized by a combination of different shapes and locations in the bi-frequency plane. Specifically, it contains a sequence of 2D planes which are different for different modulation types.

Third, we analyze the numerical SCF of pure white Gaussian noise. We ran the FAM algorithm on white Gaussian noise at power levels from -30 dB to 20 dB relative to a unit power signal and have found the SCF distributions are almost all the same as shown in Figure 4 at $\alpha \neq 0$ where the SCF is equally distributed on the bi-frequency plane and with normalized value of 0.2 . While the SCF at $\alpha = 0$ is flat and the average value increases as power level decreases.

Fourth, we use BPSK as an example and analyze its SCF at different noise levels, as shown in Figure 5. As we can see, as the SNR decreases, the SCF pattern changes.

Fifth, we also simulate Rayleigh multipath fading using the model from [24]. It is assumed that the delay power profile and the Doppler spectrum of the channel are separable and the multipath fading channel is therefore modeled as a linear finite impulse-response (FIR) filter [24]. One multipath example is shown in Figure 6 (a) and it impacts SCF pattern too. Three examples, BPSK, 8QAM, and OFDM based on QPSK signals are shown in Figure 6 (b-d) respectively.

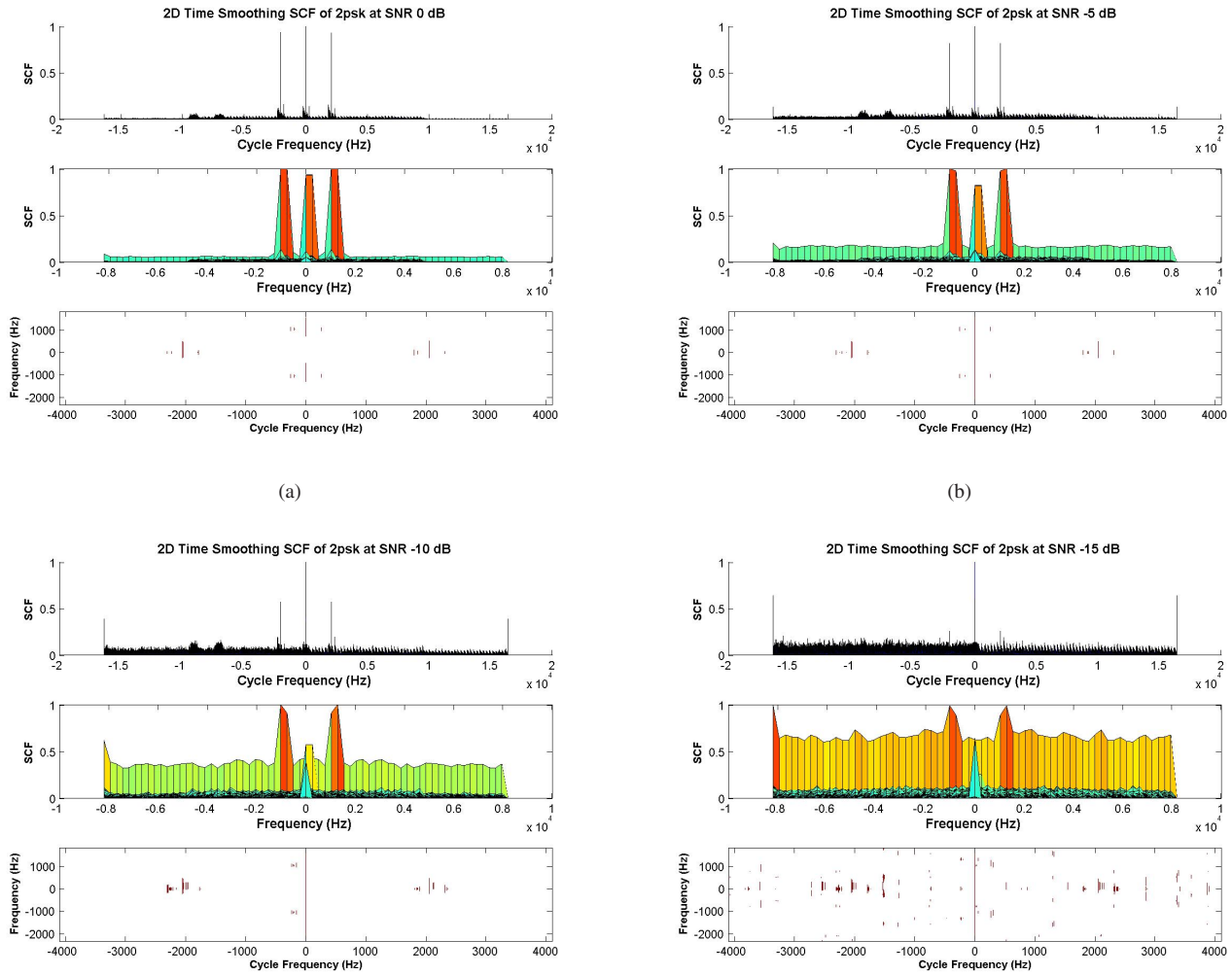

(a) (b) (c) (d)

Fig. 5. Bandlimited BPSK signal SCF under different SNR levels: (a) 0 dB; (b) -5 dB; (c) -10 dB; (d) -15 dB.

E. SCF Signal Detection Algorithm

Although different modulated signals have distinct patterns, the difference focuses on very small specific locations in the bi-frequency plane among some modulations such as QPSK, 8PSK, and QAM. Most importantly, noise and multipath together dramatically impact the SCF pattern as shown in Figure 5 and 6, which makes signal classification very challenging. In this paper we only use cyclostationary features to detect signals' existence even though we still use different modulated signals' cyclostationary features. Several detection algorithms are proposed in [25] based on spectral correlation theory.

We decouple the SCF features in the bi-frequency plane: one part corresponds to the null cycle-frequency ($\alpha = 0$) which actually represents the conventional power spectral density (PSD); the other part corresponds to the rest of the bi-frequency plane ($\alpha \neq 0$) [17]. In addition, since SCF is an even symmetric function of f and a Hermitian symmetric function of α [13]:

$$S_x^{\alpha}(-f) = S_x^{\alpha}(f)$$
$$S_x^{-\alpha}(f) = S_x^{\alpha}(f)^*$$

Therefore, we only focus on a quarter of the bi-frequency plane. In addition, as we notice in Figure 4 and 5, the noise SCF is approximately equally distributed on the plane at $\alpha \neq 0$ and its value is less than signal SCF. Therefore, we average the SCF over the entire bi-frequency plane and subtract it out of the original SCF in the first part of our detection algorithm. Next, signal SCF features consist of a series of 2D planes at discrete α values and each plane is symmetrical around a peak. Therefore, we integrate local SCF over signal frequency on such planes and average the result using the algorithm in Eq 14 (where α is constant for each plane).

$$y_{\alpha}(f) = \frac{1}{\Delta f} \int_{f-\Delta f/2}^{f+\Delta f/2} (S_x^{\alpha}(\nu) - \bar{S}_x^{\alpha}(\nu)) d\nu \qquad (14)$$

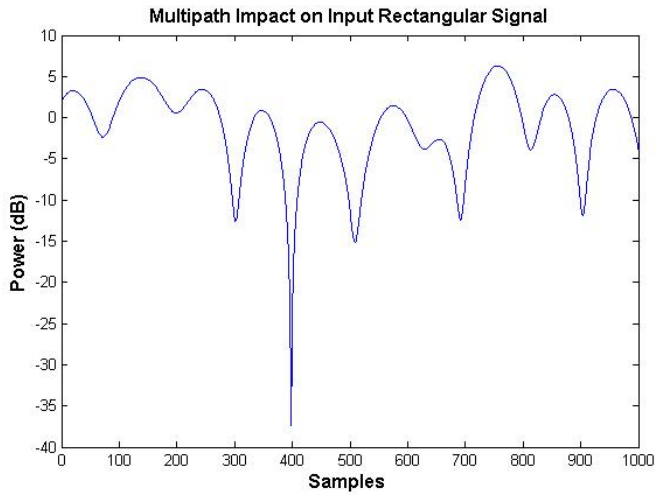

(a)

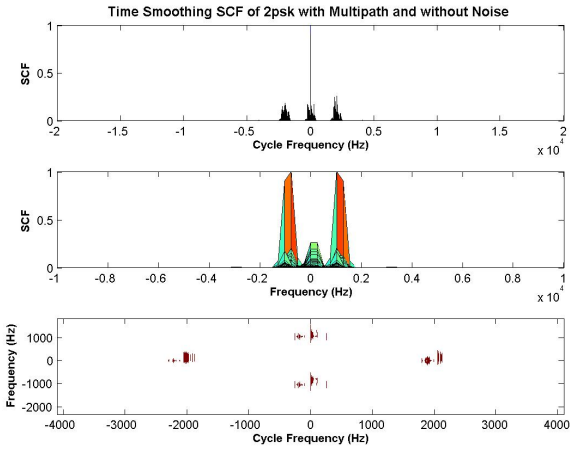

(b)

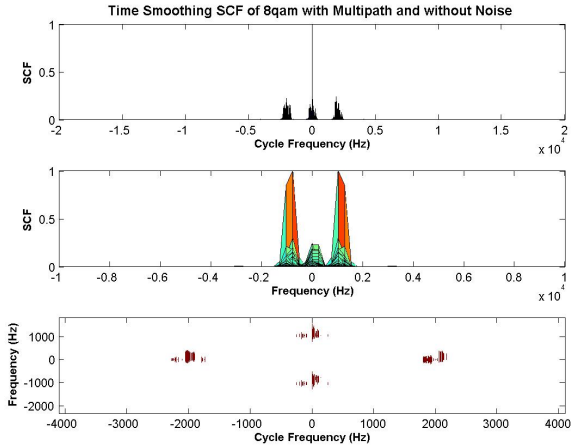

(c)

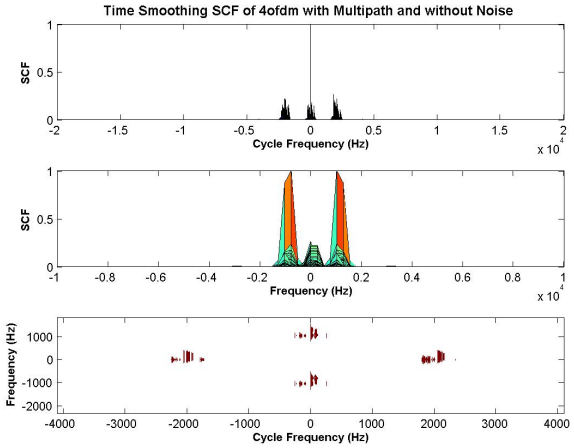

(d)

Fig. 6. (a) A multipath filter response to a rectangular signal. (b-c) Multipath impact on different signals' SCF: (b) BPSK; (c) 8QAM; (d) QPSK based OFDM.

where $y_\alpha(f)$ is a local signal SCF strength indicator in the bi-frequency plane. $\bar{S}_x^\alpha(\nu)$ is the averaged SCF value over each plane (α is constant). The integral range is decided by the following constraints:

$$(S_x^\alpha(\nu) - \bar{S}_x^\alpha(\nu)) > 0 \; over \; (f - \Delta f/2) \leq \nu \leq (f + \Delta f/2)$$
$$S_x^\alpha(\nu) \; is \; locally \; maximum \; at \; \nu = f$$

y_α can be used to detect signal's presence since it indicates local signal SCF strength. An example of y_α with $f = 0$ for QPSK signal at the carrier frequency of 2^{10} Hz and the SNR level of -20dB is shown in Figure 4.

As shown in [13], Figure 4, and Figure 5, SCF global maximum peaks happen at $(\alpha = 0, f = \pm f_c)$ and $(\alpha = \pm 2f, f = 0)$ for M-ary PSK, QAM, and continuous FSK signals (f_c is the carrier frequency). A series of local maximum peaks happens at discrete locations decided by the carrier frequency f_c and discrete α decided by symbol rate. Therefore, we can just utilize the global maximum peaks to detect signals at $\alpha \neq 0$.

The hypothesis test at f_i in Eq 1 is therefore:

$$H_1 : if \; y_\alpha(f_i) \geq \delta \; and \; f_i \; is \; a \; local \; maximum \; point$$
$$H_0 : otherwise \qquad (15)$$

where δ is decided by the noise's average SCF in the bi-frequency plane, as shown in Figure 8.

For $\alpha = 0$, the signal detection is simply a power spectrum density (PSD) detection which uses either a fixed or adaptive threshold to detect signal presence [25]. Our detection algorithm will combine both detection results made at $\alpha \neq 0$ and $\alpha = 0$.

III. Experiment Simulation and Results

In the simulation experiment, we assume that the SOI is completely unknown including its frequency and modulation type. Since most signal detection methods first down-convert signals from the RF band into an RF band, we simulate

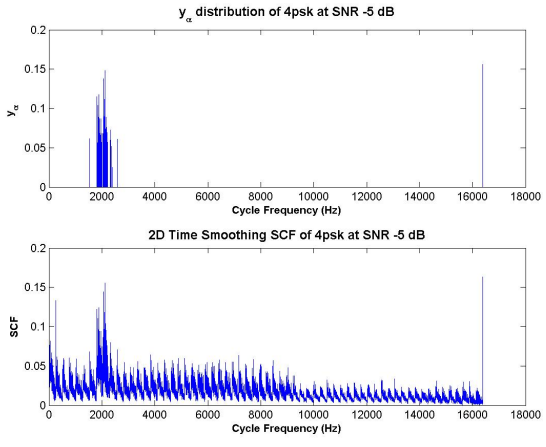

Fig. 7. An example of y_α at $f = 0$.

TABLE II
SIGNAL DETECTION PERFORMANCE ON DIFFERENT SIGNALS AT DIFFERENT SNR LEVELS.

Signals	0dB	−5dB	−10dB	−15dB	−20dB
BPSK	100%	100%	100%	95%	15%
QPSK	100%	100%	100%	80%	10%
8PSK	100%	100%	100%	90%	10%
OQPSK	100%	100%	100%	90%	10%
MSK	100%	100%	100%	90%	10%
2FSK	100%	100%	100%	95%	10%
4FSK	100%	100%	100%	95%	5%
8QAM	100%	100%	100%	95%	10%
16QAM	100%	100%	100%	95%	10%
OFDM1	100%	100%	100%	80%	5%
OFDM2	100%	100%	100%	80%	5%

different digital signals including M-ary PSK, M-ary FSK, M-ary QAM, and OFDM at an IF band. Therefore, our detection algorithm has to search the whole RF band to detect any signals' presence. In addition, all the baseband signals use root raised cosine pulse shaping before the up-conversion to the carrier frequency, which mimics pulse shaping in real communication systems. Then, we add AWGN to the signals at different SNR levels to simulate AWGN channel conditions, some examples are shown in Figure 8. Next, we add multipath fading together with different SNR levels of AWGN to simulate both noisy and fading channels. The parameter settings for signal simulation are: the sampling frequency is 16384Hz, the RF carrier frequency is 1024Hz, the FSK's frequency separation is 100Hz, the OFDM block size is 16 and its cyclic prefix is 7, the pulse shaping filter roll-off is 0.25, and the filter order is 32.

TABLE III
SIGNAL DETECTION PERFORMANCE ON DIFFERENT SIGNALS AT DIFFERENT SNR LEVELS WITH MULTIPATH FADING.

Signals	0dB	−5dB	−10dB	−15dB	−20dB
BPSK	100%	100%	100%	85%	10%
QPSK	100%	100%	100%	75%	5%
8PSK	100%	100%	100%	75%	5%
OQPSK	100%	100%	100%	75%	10%
MSK	100%	100%	100%	75%	10%
2FSK	100%	100%	100%	85%	5%
4FSK	100%	100%	100%	80%	5%
8QAM	100%	100%	100%	90%	10%
16QAM	100%	100%	100%	70%	5%
OFDM1	100%	100%	100%	90%	10%
OFDM2	100%	100%	100%	90%	5%

To detect the signals, first we run the FAM algorithm to get their SCF value in the bi-frequency plane. Then, we calculate the SCF's magnitude and normalize it to the range $[0, 1]$. Therefore, our signal detection algorithm is based on real positive values within 0-1. Next, we use the detection algorithm shown in Eq 14 and estimate any signal's existence subject to Eq 15. In addition, we also find the centers of dense clusters like what is shown in Figure 7 and use the cluster centers to estimate the carrier frequencies. We are able to do so because SCF global maximum peaks happen at $(\alpha = 0, f = \pm f_c)$ and $(\alpha = \pm 2f, f = 0)$ for M-ary PSK, QAM, and continuous FSK signals (f_c is the carrier frequency). This estimation is also confirmed in the plane of $\alpha = 0$ which is a PSD detection problem. The parameter settings for the FAM and signal detection algorithm are: $N' = 64$, $P = 1024$, and $L = 8$, $\delta = 0.05$.

For pure AWGN channel, the detection of signal existence for 20 rounds of simulation is shown in Table II, where OFDM1 and OFDM2 represent OFDM based on BPSK and QPSK respectively. As we can see, the signal detection algorithm does not have any missing error until SNR drops to -15dB, and it doesn't have any statistical meaning at -20dB SNR at current algorithm parameter settings.

Next, we simulate both AWGN and Rayleigh multipath fading channel. The parameter setting for Rayleigh multipath fading simulation is: the sample time of the input signal $t_s = 1/16384$ s, the maximum Doppler shift $f_d = 100Hz$. They are for the frequency-flat ("single path") Rayleigh fading channel simulation parameters. For frequency-selective ("multiple path") fading channel, we use six paths with the vector of path delays of $[0, 1.2, 2.3, 6.2, 11.3, 15.4] * t_s$ and the corresponding path gains are linearly related to the path delay. The signal detection result for 20 rounds of frequency-selective fading simulation is shown in Table III. As we can see, the detection performance is almost the same with the result only under AWGN channels except that the missing error is higher at -15dB SNR.

IV. CONCLUSION AND DISCUSSION

In this paper, we design a parallel algorithm based on a Cell BE to attack the high computation requirement in calculating cyclostationary feature. We also design a spectrum sensing algorithm which uses the distinct SCF pattern of modulated signals to detect their existence. We run this algorithm on simulated signals including M-ary PSK, FSK, QAM, and PSK based OFDM under conditions of multipath fading and different SNRs. We analyze the impact of AWGN and Rayleigh multipath fading on signals' SCF features in the bi-frequency plane by giving numerical results.

As discussed in [26], there exist SNR walls for feature detectors though the relative locations of the SNR walls differ for different algorithms. It is also important to exploit the exact location for a specific feature detector such as the cyclostationary feature detection described here. Our experiment verifies the existence of an SNR wall for cyclostationary feature detection. Besides, our result shows that multipath has an impact too.

In the experiment, we use a finite number of samples in the SCF calculation. This influences the way that noise impacts the final SCF [22]. In addition, there are other limitations of spectral correlation based detectors [17]. Our future research will explore the sample duration and other limitations. We will also analyze the detector's ROC curve under different parameters.

To attack the possible computation for larger numbers of samples, we will use more SPEs at the task parallelism level and use other Cell BE programming techniques like multi-buffering instead of double-buffering, loop unrolling for reducing dependencies, dual issue pipeline, etc.

ACKNOWLEDGMENT

This work was supported by DARPA under grant W31P4Q-07-C-0210, by the National Institute of Justice, Office of Justice Programs, U.S. Department of Justice under Award No. 2005-IJ-CX-K017, and by the National Science Foundation under Grant No. CNS-0519959. The opinions, findings, and conclusions or recommendations expressed are those of the authors and do not necessarily reflect the views of these sponsors or the official policy or position of the DARPA, Department of Defense, or the U.S. Government.

REFERENCES

[1] I. F. Akyildiz, W. Y. Lee, M. C. Vuran, and S. Mohanty, "Next generation/dynamic spectrum access/cognitive radio wireless networks: a survey," *Computer Networks: The International Journal of Computer and Telecommunications Networking*, vol. 50, pp. 2127–2159, 2006.

[2] S. D. Meinrath and M. Calabrese, "Unlicensed broadband device technologies: 'white space device' operations on the tv band and the myth of harmful interference," New America Foundation: Policy Backgrounder.

[3] S. M. Mishra, A. Sahai, and R. W. Brodersen, "Cooperative sensing among cognitive radios," in *IEEE International Conference on Communications*, 2006, pp. 1658–1663.

[4] W. A. Gardner and C. M. Spooner, "Signal interception: performance advantages of cyclic-feature detectors," *IEEE Trans. Commun.*, vol. 40, no. 1, pp. 149–159, 1992.

[5] J. A. Kahle, M. N. Day, H. P. Hofstee, C. R. Johns, T. R. Maeurer, and D. Shippy, "Introduction to the cell multiprocessor," *IBM Journal of Research and Development*, vol. 49, pp. 589–604, 2005.

[6] M. Gschwind, "The cell broadband engine: Exploiting multiple levels of parallelism in a chip multiprocessor," *International Journal of Parallel Programming*, vol. 35, pp. 233–262, 2007.

[7] R. S. Roberts and J. H. H. Loomis, "Parallel computation structures for a class of cyclic spectral analysis algorithm," *Journal of VLSI Signal Processing*, vol. 10, pp. 25–40, 1995.

[8] A. C. Chow, G. C. Fossum, and D. A. Brokenshire, "A programming example: Large fft on the cell broadband engine," Global Signal Processing Expo (GSPx) Santa Clara, California, 2005.

[9] R. O. Duda, P. E. Hart, and D. G. Stork, *Pattern Classification*. Wiley-Interscience, Second edition, 2000.

[10] J. Proakis, *Digital Communications*. McGraw-Hill Science/Engineering/Math; 4 edition, 2000.

[11] W. A. Gardner, A. Napolitano, and L. Paura, "Cyclostationarity: Half a century of research," *Journal of Signal Processing*, vol. 86, no. 4, 2006.

[12] R. S. Roberts, W. A. Brown, and J. H. H. Loomis, "Computationally efficient algorithms for cyclic spectral analysis," *IEEE Signal Processing Magazine*, vol. 8, pp. 38–49, 1991.

[13] W. A. Gardner, *Statistical spectral analysis: a nonprobabilistic theory*. Prentice-Hall, 1988.

[14] N. J. Carter, "Implementation of cyclic spectral analysis methods," Master Thesis, Naval Postgraduate School, 1993.

[15] F. Ge and C. W. Bostian, "A wide band spectrum sensing approach with agility and low snr sensitivity," Software Defined Radio Technical Conference, Denver, Colorado, November, 2007.

[16] E. L. d. Costa, "Detection and identification of cyclostationary signals," Master Thesis, Naval Postgraduate School, 1996.

[17] O. A. Yeste-Ojeda and J. Grajal, "Limitations of spectral correlation based detectors," in *IEEE/SP 14th Workshop Statistical Signal Processing*, 2007, pp. 244–248.

[18] J. Hennessy and D. Patterson, *Computer Architecture A Quantitative Approach*. Morgan Kaufmann, Fourth edition, 2006.

[19] D. H. Bailey, "A high-performance fast fourier transform algorithm for the cray-2," *The Journal of Supercomputing*, vol. 1, pp. 43–60, 1987.

[20] K. Kim, I. Akbar, K. Bae, J. Urn, C. Spooner, and J. Reed, "Cyclostationary approaches to signal detection and classification in cognitive radio," in *2nd IEEE International Symposium on New Frontiers in Dynamic Spectrum Access Networks (DySPAN)*, 2007, pp. 212–215.

[21] W. C. Headley, J. Reed, and C. R. C. M. da Silva, "Distributed cyclic spectrum feature-based modulation classification," in *Proc. IEEE Wireless Comm. and Netw. Conf.*, 2008, pp. 1200–1204.

[22] P. Sutton, K. Nolan, and L. Doyle, "Cyclostationary signatures for rendezvous in ofdm-based dynamic spectrum access networks," in *2nd IEEE International Symposium on New Frontiers in Dynamic Spectrum Access Networks (DySPAN)*, 2007, pp. 220–231.

[23] P. Sutton, J. Lotze, K. Nolan, and L. Doyle, "Cyclostationary signature detection in multipath rayleigh fading environments," in *2nd International Conference on Cognitive Radio Oriented Wireless Networks and Communications (CROWNCOM)*, 2007, pp. 220–231.

[24] M. C. Jeruchim, P. Balabanand, and K. S. Shanmugan, *Simulation of Communication Systems, Second Edition*. New York, Kluwer Academic/Plenum, 2000.

[25] W. A. Gardner, "Signal interception: A unifying theoretical framework for feature detection," *IEEE Transactions on Communications*, vol. 36, no. 8, 1988.

[26] R. Tandra and A. Sahai, "Snr walls for feature detectors," in *1nd IEEE International Symposium on New Frontiers in Dynamic Spectrum Access Networks (DySPAN)*, 2005, pp. 559–570.

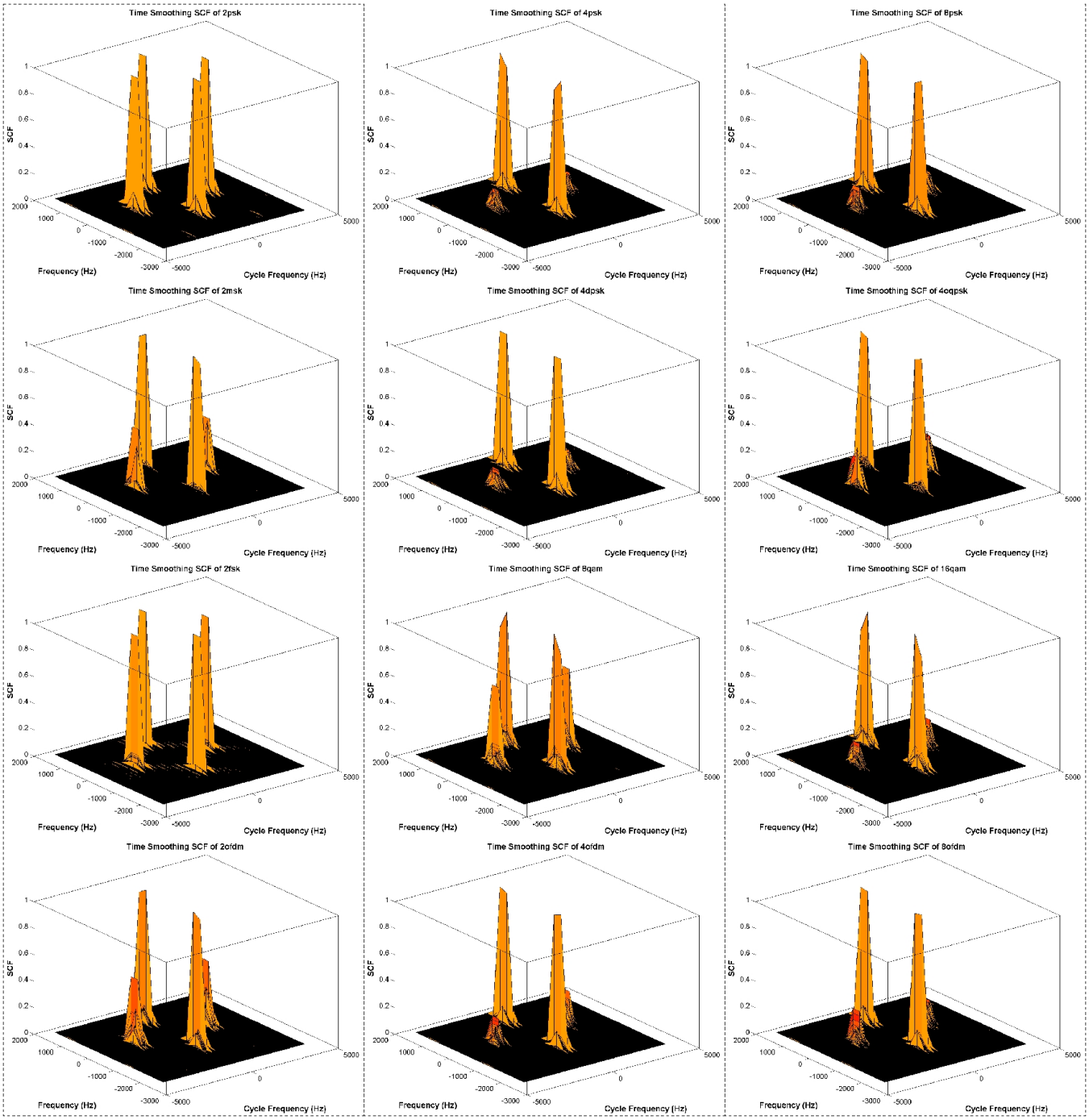

Fig. 8. SCF of different modulated signals.